Effects of working pressure on structure and properties of Al-containing amorphous carbon films prepared by high-power impulse magnetron sputtering

Ya-Li Peng [a,b], Chao-Qian Guo [b,*], Song-Sheng Lin [b], Qian Shi [b], Chun-Bei Wei [b], Yi-Fan Su [b], Yi-Qian Wu [b,c], Peng Tang [b], Xia-Gao Zhu [b], Ming-Jiang Dai [b,**]

[a] School of Materials Science and Engineering, Central South University, Changsha, 410083, China
[b] Guangdong Institute of New Materials, National Engineering Laboratory for Modern Materials Surface Engineering Technology, The Key Lab of Guangdong for Modern Surface Engineering Technology, Guangzhou, 510651, China
[c] School of Material Science and Engineering, South China University of Technology, Guangzhou, 510640, China

ARTICLE INFO

ABSTRACT

Al-containing amorphous carbon (a-C:Al) films were fabricated under different working pressures by high-power impulse magnetron sputtering. Morphologies, microstructure and chemical composition of a-C:Al films were characterized by scanning electron microscopy, atomic force microscope, X-ray photoelectron spectroscopy, transmission electron microscopy and Raman spectroscopy. Mechanical properties and tribological behavior of a-C:Al films were investigated by film stress tester, nano-indentation, scratch tester, ball-on-disk tribometer and 3D surface profiler. Results showed that atomic composition of Al in a-C:Al films was about 5%, independent of working pressure. The prepared films have smooth surfaces with Ra of 2.22 nm–5.89 nm. Typical amorphous structures could be observed in a-C:Al films and sp^3 content could be governed by changing working pressures. Al existed as an oxide of aluminum in carbon matrix. There was a notable negative correlation between internal stress and sp^3-C content. All samples manifested good adhesion strength to substrates with critical loads beyond 70 N. Wear rates were in $10^{-8} mm^3 N^{-1} m^{-1}$ order of magnitude and had the same changing trend with H/E as working pressure rose from 0.3 Pa to 0.6 Pa. a-C:Al film prepared at 0.4 Pa has the best wear resistance with a wear rate of $4.38 \times 10^{-8} mm^3 N^{-1} m^{-1}$.

© 2019

1. Introduction

Amorphous carbon (a-C) films can be widely used in the fields of machinery, optics, electronics and biomedicine due to its excellent properties such as high hardness and elastic modulus, low friction coefficient, superior wear resistance, high chemical stability and great biocompatibility [1–4]. On the other hand, drawbacks are apparent when using a-C films, like high internal stress and poor adhesion to substrates [5–9]. Over the past few decades, numbers of studies have revealed that Al doping of a-C films (a-C:Al) can reduce internal stress and improve the mechanical and tribological suitability of a-C films effectively [10,11]. Xu et al. [12] studied the structures and properties of Al-doped diamond-like films at various bias voltages. Results showed that doping of Al can regulate the internal stress of films extraordinarily, which changed from compressive stress to tensile stress. Dai et al. [13] prepared Al-containing diamond-like carbon films by magnetron sputtering technology and found that the films exhibited a lower friction coefficient than pure diamond-like carbon films. However, most of the re-

ported a-C:Al films are hydrogenated. Cathodic vacuum arc deposition and magnetron sputtering are common methods for preparing hydrogen-free a-C films while both of the two technologies have limitations (pollution of macroparticles or low ionization) [14,15]. High-power impulse magnetron sputtering (HiPIMS) as a new type of magnetron sputtering technology with stable discharge and high ionization rate has become widely used in film preparation [16–18]. Nevertheless, few studies on hydrogen-free a-C:Al films deposited by HiPIMS have been reported.

Properties and structures of thin films are strongly influenced by deposition parameters, especially working pressure. Nakao et al. [19] studied the effects of working pressure on microstructure of diamond-like carbon (DLC) films prepared by high-power impulse magnetron sputtering. It suggested that the DLC film's density and the content of sp^2 bonds varied with the change of working pressure. Andujar et al. [20] found that the increase of working pressure leads to scattering and thermalization of sputtered carbon atoms, reducing film deposition rate, compressive stress, and quantity of ordered sp^2 phase. Hence, structures and properties of a-C films can be effectively adjusted by changing working pressure.

In this paper, a-C:Al films were fabricated by HiPIMS using a C–Al composite target and effects of working pressure were studied on composition, microstructure, mechanical and tribological properties of a-C:Al films.

* Corresponding author.
** Corresponding author.
    E-mail addresses: cqguo12s@alum.imr.ac.cn (C-Q Guo); daimingjiang@tsinghua.org.cn (M-J Dai)

2. Experimental details

2.1. Film deposition

a-C:Al films were prepared on (100) single crystal silicon wafers and YG6 cemented carbides by HiPIMS under different working pressures. Film deposition equipment shown in Fig. 1 is a kind of scientific research multi-functional coating machine, consisting of a self-made C–Al target (Al rods inlaid in graphite target, 99.99%) with a high-power impulse power and a Cr target (99.99%) with direct-current power. Substrates were ultrasonically cleaned with acetone and alcohol for 15 min respectively, dried by hot air, and then placed in a vacuum chamber which was evacuated to 1.0×10^{-3} Pa later. Before preparing the film, substrates were sputtered with Ar plasma for 30 min at a bias voltage of −400 V to remove residual contaminants on substrates' surface. To enhance the adhesion strength between a-C:Al films and substrates, Cr/ Cr_xAl_yC gradient transition layers were deposited. Sets of a-C:Al films were obtained under different working pressures (0.3 Pa, 0.4 Pa, 0.5 Pa, and 0.6 Pa) by changing Ar gas flow rate (100 sccm, 130 sccm, 165 sccm, 195 sccm). When Cr/Cr_xAl_yC transition layer was prepared, substrates holder rotated with a speed of 2 rpm and then substrates holder stopped to keep substrates facing the C–Al target to deposit a-C:Al layer. The distance between target and substrates was 8 cm. During the deposition process, temperature of the vacuum chamber was kept at 80 °C and substrates' negative bias voltage was 200 V with duty ratio of 80% and ion source with the current of 1.5 A was used to assist film deposition. The pulse power of C–Al target was 3 kW with duty ratio of 15%. The deposition time was 120 min.

2.2. Film characterization

3D surface profiler (Dektak-XT, Bruker) was used to determine the thicknesses of films through steps formed by shadow masks. Surface and cross-section morphologies of a-C:Al films were characterized by scanning electron microscope (SEM, SU8220, HITACHI) with energy-dispersive X-ray spectroscopy (EDS) and atomic force microscope (AFM, Bruker Dimension edge), respectively. X-ray photoelectron spectroscopy (XPS, Escalab 250Xi) was employed to analyze the electron binding energy and film composition. The sample surface was etched using an Ar^+ ion beam with energy of 3 keV for 60 s to remove oxides and contaminants before the measurement. Transmission electron microscope (TEM, FEI Talos F200) was used to characterize microstructure of films. The bonding structure of carbon atoms was analyzed by means of Raman spectroscopy (Horiba Scientific, Xplora Plus) with an excitation wavelength of 532 nm.

With a film stress tester (FST150, SuPro), residual stresses of a-C:Al films were obtained through measuring the radius of curvature of silicon wafers with a thickness of $400 \pm 10 \mu m$ before and after film deposition according to Stoney equation [21–23]. Nano-indentation tester (NHT3, Anton Parr) with a Berkovich diamond tip was adopted to investigate a-C:Al films'
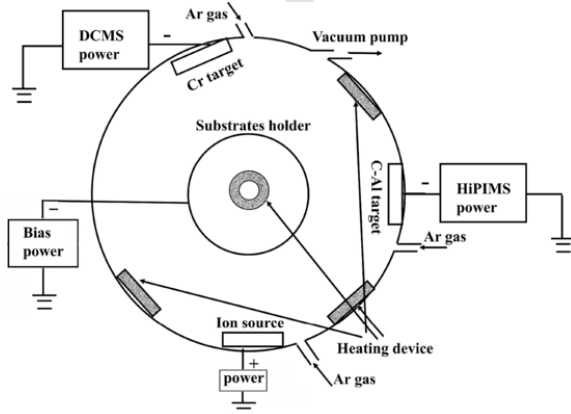
hardness and elastic modulus. In order to minimize the substrate effect, indentation depth should be less than 1/10 of the film thickness. scratch tester (MFT-4000) was used to measure the adhesion strength between films and substrates. Normal load was gradually increased from 0 N to 100 N at a rate of 100 N/min, and the scratch length was 5 mm. Tribological behavior of a-C:Al films were analyzed in an ambient atmosphere with a ball-on-disk tribometer (MS-T3001) at a relative humidity of 50% ± 5%. All friction tests were carried out under a normal load of 5 N with a sliding speed of 0.2 m/s for 120 min and steel balls (GCr15, 4 mm) were used as the counterpart. After friction tests, wear tracks on a-C:Al films and wear scars on steel balls were characterized by SEM, Raman, and XPS. Wear rates were calculated according to the Archard equation through measuring profiles of wear tracks by 3D surface profiler.

3. Results and discussion

3.1. Thickness and composition

Table 1 shows the thickness, deposition rate and atomic composition of a-C:Al films deposited at different working pressures. It can be seen that thickness and deposition rate of a-C:Al films both increased monotonously with working pressure rising from 0.3 Pa to 0.5 Pa. Lin et al. [24] think that the increased ion current to target due to more collisions of microparticles and the declined ion bombardment to film surface caused by much shorter mean free path of ions contribute to the rise of deposition rate. Within a certain range, the increase of working pressure leads to a higher deposition rate. As working pressure increased from 0.5 Pa to 0.6 Pa film thickness decreased from 1265 nm to 1149 nm. Accordingly, deposition rate declined from 10.5 nm/min to 9.6 nm/min. With the growth of working pressure, the probability of collisions between particles sputtered from target and ions or atoms of Ar ascended and the scattering effect was significantly improved as well. Then the number of sputtered atoms and ions reaching film's surface was expected to fall. As a result, a-C:Al film prepared at 0.6 Pa is much thinner than the film prepared at 0.5 Pa. In addition, what stands out in this table is that the atomic concentrations of different a-C:Al films are similar, which means the chemical composition of a-C:Al films are almost independent of working pressure.

3.2. Morphology

Fig. 2 depicts cross-sectional morphologies of a-C:Al films prepared at various working pressures. All films have a similar structure that includes Cr/Cr_xAl_yC transition layer and a-C:Al layer. The a-C:Al films have a dense and amorphous structure without obvious grain boundaries. To understand the elemental distribution in a-C:Al film, the cross-sectional morphology and the corresponding EDS mapping images of a-C:Al film fabricated at 0.5 Pa was demonstrated in Fig. 3. Fig. 3(b) and (c) display that the outer layer mainly consists of C and Al elements, together with a small number of O elements, which is consistent with the atomic composition shown in Table 1. Fig. 3(d) displays that the main element of transition layer is Cr, and the upper part of it has the presence of C and Al elements. It is noteworthy that oxygen is enriched in Cr/Cr_xAl_yC transition layer in Fig. 3(e). Be-

Fig. 1. Schematic of film deposition equipment.

Table 1
Thickness, deposition rate and compositions of a-C:Al films deposition at different working pressures.

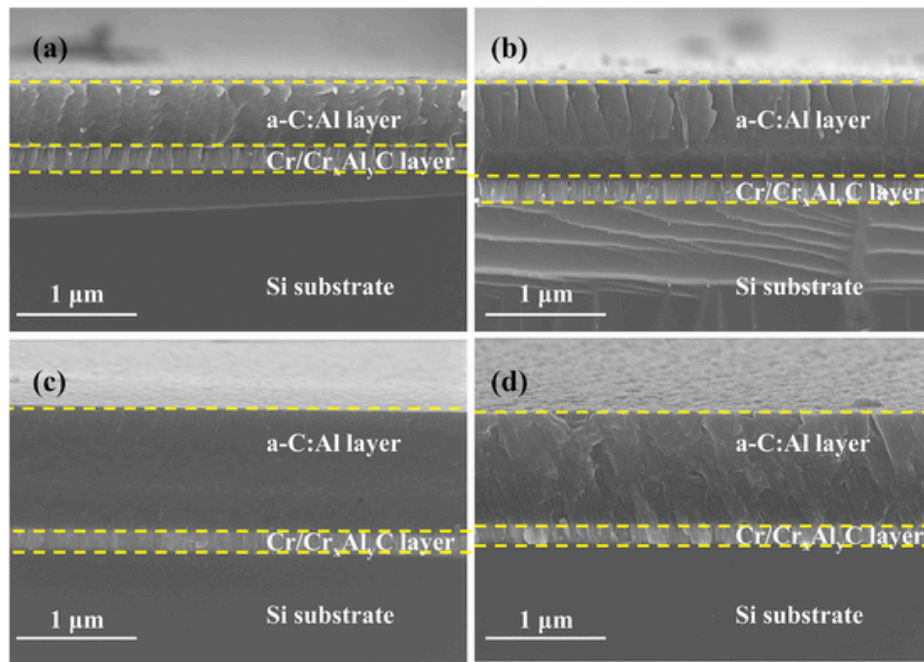| Working pressure (Pa)	Thickness (nm)	Deposition rate (nm/min)	Atomic composition (at.%)		
			C	Al	O
0.3	636	5.30	85.56	6.03	8.41
0.4	976	8.13	85.52	4.93	9.55
0.5	1265	10.54	88.95	5.67	5.38
0.6	1149	9.58	90.48	4.61	4.90

Fig. 2. SEM cross-sectional images of a-C:Al films at different working pressures: (a) 0.3 Pa, (b) 0.4 Pa, (c) 0.5 Pa, (d) 0.6 Pa.
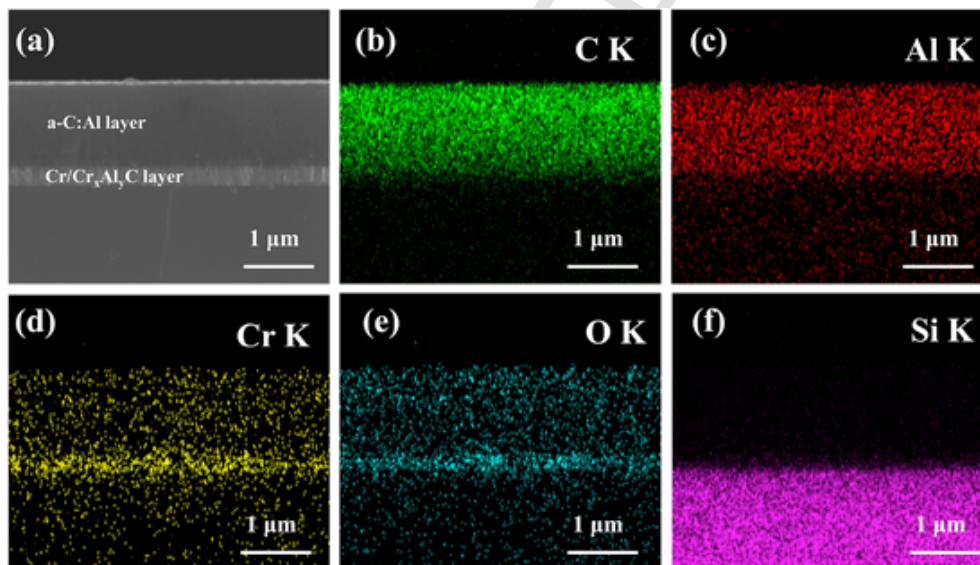

Fig. 3. (a) Cross-sectional SEM morphology of a-C:Al deposited at 0.5 Pa and corresponding EDS mapping for (b) C, (c) Al, (d) Cr, (e) O and (f) Si.

fore SEM characterization, the cross-sectional area of the film contacted with air. ΔG_f of Cr reacting with oxygen is much lower than that of C reacting with oxygen at room temperature [25]. That means oxygen is more likely to react with Cr rather than C, resulting that O concentrated in Cr/Cr_xAl_yC transition layer.

Fig. 4 presents the surface morphologies of a-C:Al films. Films' surfaces are smooth and dense except that the one at 0.6 Pa has numerous hillocks, similar to "cauliflower". Combined with surface morphologies, roughness (Ra) of a-C:Al films are presented in Fig. 4(e–h) a-C:Al films prepared at low working pressure (0.3–0.5 Pa) are relatively smooth and surface roughnesses are at a low level (2.22 nm-3.30 nm) while Ra of film fabricated at high working pressure (0.6 Pa) have a maximum value of 5.98 nm. Surface diffusion of adatoms and etching or erosions of energetic ions could contribute to smoothening of growing film surface [26,27]. Compared with the deposition process under high working pressure, a large number of C ions and Al ions had fewer chances of impacting with Ar^+ at low working pres-

sure, which caused high energy spices to bombard film surface and boosted atoms diffusion. As working pressure rose to 0.6 Pa, the increase of Ar or Ar^+ particles and the scattering of sputtered atoms resulted in an increase of tilting velocity component and a decrease of average kinetic energy of the sputtered atoms [28]. Both factors promoted the island-like growth of a-C:Al film, which caused high roughness.

3.3. Microstructure

To study the chemical states of carbon and aluminum, a-C:Al film deposited at 0.4 Pa was characterized by XPS. Fig. 5(a) displays a-C:Al film's typical XPS survey scan and it consists of C, Al, and O, consistent with the results of EDS. Fig. 5(b) reveals that C1s spectrum could be deconvoluted into three peaks around 284.1 eV, 284.7 eV, 286.1 eV corresponding to sp^2-C, sp^3-C, and C–O, respectively [29,30]. Al–C–O   peak   (nearly   282.5 eV)   and
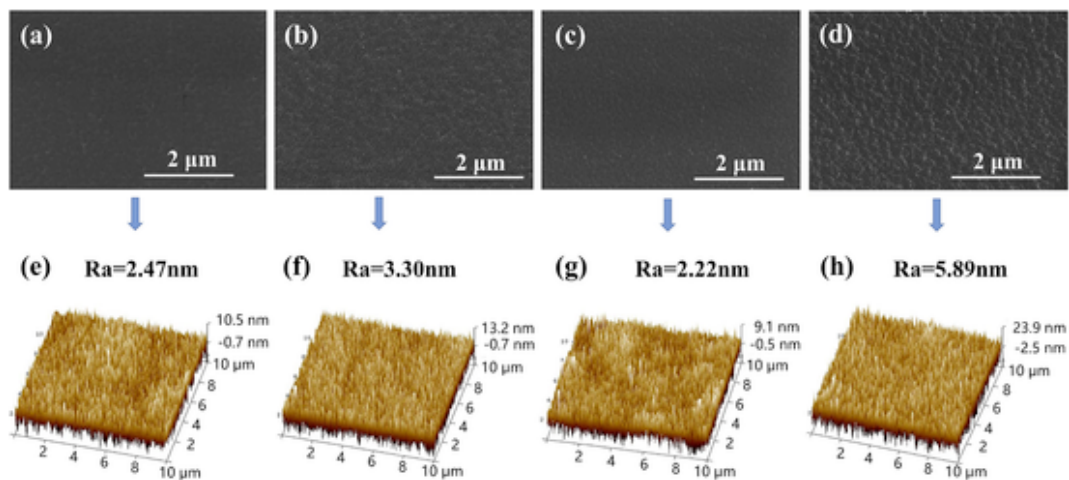
Fig. 4. (a)~(d) SEM surface morphologies and (e)~(h) AFM images and the RMS surface roughness of the a-C:Al films deposited at different working pressures: (a), (e) 0.3 Pa; (b), (f) 0.4 Pa; (c), (g) 0.5 Pa; (d), (h) 0.6 Pa.
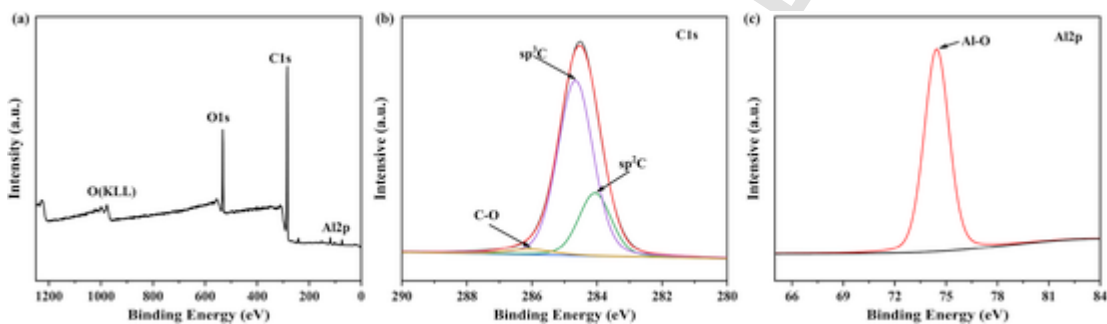

Fig. 5. XPS spectra of a-C:Al film deposited at 0.4 Pa: (a) survey scan spectrum, (b) C1s fitting spectrum, (c) Al2p fitting spectrum.

Al–C (nearly 281.5 eV) peak were undetected, suggesting that C didn't react with Al [31,32]. Fig. 5(c) depicts that the peak of Al2p was located at about 74.7 eV representing Al–O bond, which means doped Al existed as oxidized aluminum. This is consistent with some other researches [33,34]. The decomposition of O_2 or H_2O remained in the vacuum chamber was a key factor in the formation of oxidized aluminum during the HiPIMS deposition process.

Results of TEM characterization for a-C:Al film deposited at 0.4 Pa are presented in Fig. 6. Si substrate, dark Cr/Cr_xAl_yC transition layer, and grey a-C:Al layer can be clearly distinguished in Fig. 6(a) which is the film's cross-sectional image measured by high-angle annular dark field scanning transmission electron microscopy (HAADF-STEM). A mixed zone with the thickness of several nanometers at the interface between Cr layer and Si substrate could be observed in Fig. 6(b) probably caused by Ar ion bombardment before film deposition. Cr grew on silicon surface with a damaged crystalline structure and generated the amorphous-like mixed zone. The crystalline structure of Cr_xAl_yC layer grew gradually to the amorphous structure of a-C:Al layer without an obvious interface as shown in Fig. 6 (c). The gradient change in microstructure or composition from substrate to transition layer and a-C:Al film which can reduce the interfacial free energy, decrease the mismatch and lower physical properties difference between different materials which is beneficial to improve adhesion strength [5,35]. Fig. 6(d) illustrates TEM micrograph and corresponding selected area electron diffraction (SAED) pattern of a-C:Al layer. It was found that the high-resolution image exhibited a dense and amorphous structure and corresponding SAED image displays a broad and diffuse diffraction halo in the insert image, indicating a typical amorphous feature of a-C:Al film. To figure out the existence of Al in carbon matrix further, the HAADF-STEM combined with energy-dispersive X-ray spectrometry was used. It can be observed from Fig. 6(f) that the elements of C, Al, and O changed slightly as scan-

ning position altered shown in Fig. 6(e). The two vertical lines (1 and 2) in Fig. 6(f) corresponding to the two points in Fig. 6(e) at which contents of Al and O had peak values while content of C fell to low values illustrated that Al and O were concomitant. This agrees with the result of XPS that Al existed as oxidized aluminum in carbon matrix. Apparently, some dark areas could be seen in Fig. 6(e) which maybe contaminations induced by ion milling for TEM specimen preparation.

Typical Raman spectrum of DLC film has a D peak and a G peak in the range of 1000 cm^{-1} to 1800 cm^{-1} [36,37]. Fig. 7(a) manifests Raman spectra of a-C:Al films at different working pressures. There exist D peaks around 1350 cm^{-1} and G peaks around 1550 cm^{-1}. D peak is associated with breathing vibration of sp^{2}C–C in full six-membered carbon rings, while G peak is attributed to the stretching vibration of sp^{2}C–C in benzene rings and olefinic chains carbon [38,39]. What is more, the intensity ratio of D peak to G peak (I_D/I_G), the position of G peak and the full width at half maximum of G peak (G_{FWHM}) reflect DLC film's microstructure information such as the value of sp^3-C/sp^2-C and structural disorder in the DLC film [40]. Fig. 7 (b) presents that with the increase of working pressure, I_D/I_G displays a trend of falling at first and then rising. The climbing value of I_D/I_G means the increase of graphitic component in a-C:Al film. As working pressure rose from 0.3 Pa to 0.4 Pa the number of carbon ions increased. Subplantation of carbon ions with certain energy increased the density of adjacent micro-region to some extent, which gave rise to an adjustment of the chemical bonding of relative atoms and generated more sp^3 bonding [41,42]. And then, as working pressure ascended, energy of carbon ions reduced due to collisions with ions or atoms of Ar and sp^3 content in a-C:Al film declined. It can be seen in Fig. 7(c) that positions of G peaks of the four samples change slightly while G_{FWHM} goes up first and then goes down, which presents ordering and graphitizing of films [43]. Thus, a-C:Al film deposited at 0.4 Pa
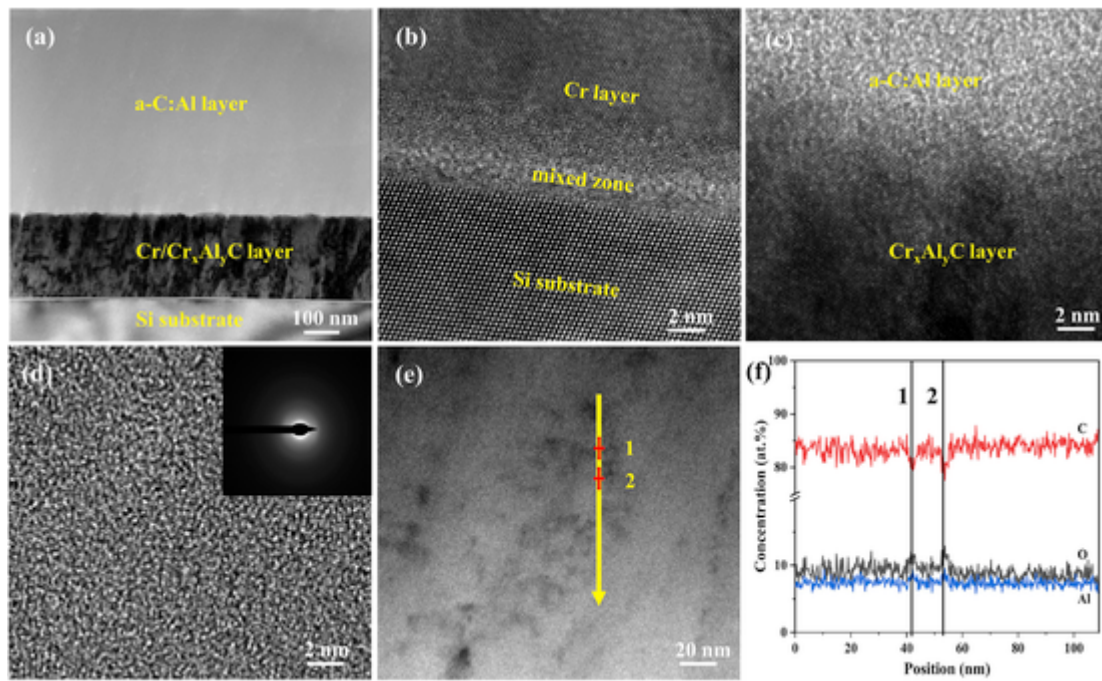
Fig. 6. (a) Cross-sectional HADDF-STEM image micrograph of a-C:Al film prepared at 0.4 Pa; (b) HRTEM image of interface between Si substrate and Cr layer; (c) HRTEM image of interface between Cr_xAl_yC layer and a-C:Al layer; (d) a-C:Al film's HRTEM image and corresponding SAED pattern; (e) HADDF-STEM image of a-C:Al film; (f) line-scan EDX analysis along the yellow line in the Fig. 6(e). (For interpretation of the references to colour in this figure legend, the reader is referred to the Web version of this article.)
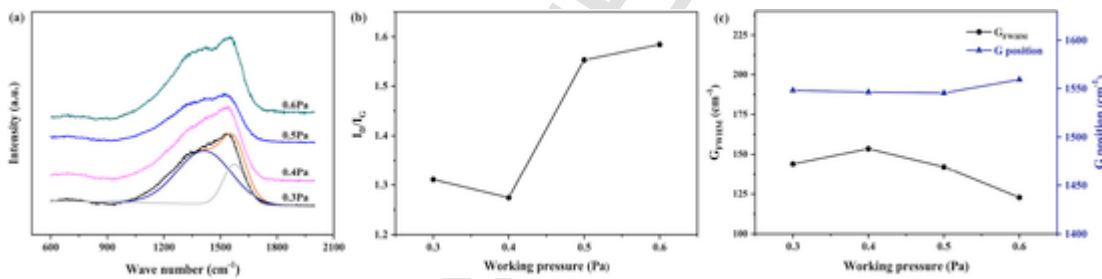

Fig. 7. (a) Raman spectra; (b) the corresponding I_D/I_G and (c) G_{FWHM} and G peak position of a-C:Al films deposited at different working pressures.

has the highest G_{FWHM} (153.49 cm^{-1}) and the lowest I_D/I_G (1.27), demonstrating it possesses the best ordered and highest sp^3-C fraction.

3.4. Mechanical properties

Fig. 8 presents residual stress of a-C:Al films as a function of working pressure. Residual stresses in a-C:Al films are still at a high level (−2.00~-2.50 GPa) which was somewhat counterintuitive with most studies, in which it has been greatly reduced by Al doping [13,33,44]. Probably, the low Al content of about 5 at.% and the oxide of aluminum in a-C:Al film are responsible for the high compressive stress. Some researchers suggested that the cause of high internal stress would be the formation of sp^3-C in the early stage of film growth [45,46]. However, taking the sp^3 content of each sample into consideration, it could be known that there was no particular correlation between sp^3 content and residual stress. The a-C:Al film prepared at 0.4 Pa with the highest sp^3-C content has the lowest internal stress (−1.98 GPa). Hence, internal stress is an unnecessary condition for the high-stability sp^3-C in DLC films [47].

Fig. 9 displays hardness (H), elastic modulus (E) and, H/E and H^3/E^2 of a-C:Al films deposited under different working pressures. As Fig. 9(a) describes, hardness and elastic modulus of a-C:Al film at 0.4 Pa rose to a high point and peaked in 16.62 GPa and 200.44 GPa respectively. It is well known that hardness of DLC films is increased with the growth of sp^3-C content [48]. Based on Raman spectroscopy results mentioned above, within a cer-
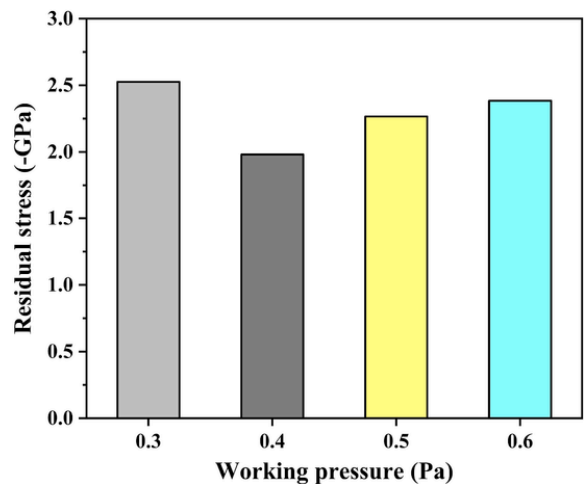

Fig. 8. Residual stress of a-C:Al films at different working pressures.

tain range, the trend of hardness is basically identical to that of sp^3-C content in films. However, as for the film fabricated at 0.6 Pa, which has the lowest sp^3-C content and G_{FWHM}, its hardness and elastic modulus increased to 15.68 GPa and 204.32 GPa, respectively. This may be related to three-dimensional sp^2-rich structures [49]. The disorder of bond angles in sp^2 bond
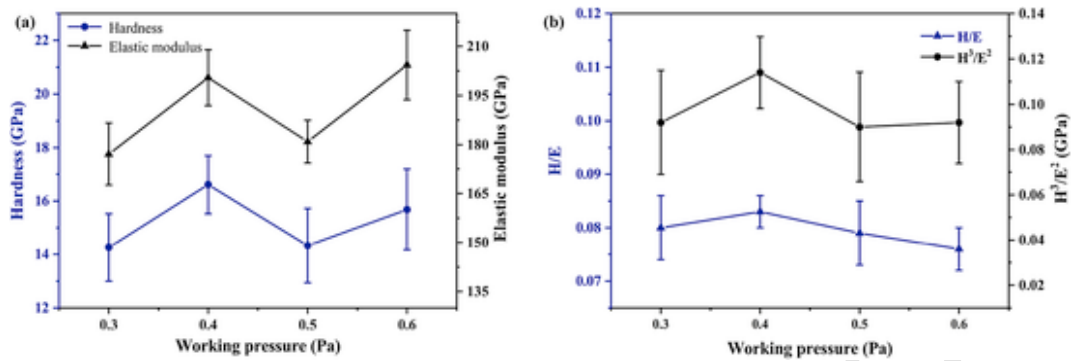
Fig. 9. (a) H, E and (b) H/E, H^3/E^2 of a-C:Al films deposited at different working pressures.

structure promotes the formation of a non-six-membered ring structure, thereby forming a curved three-dimensional structure. In this condition, the three-dimensional network structure in which σ bond is connected can also exhibit a high hardness. Accordingly, it can be firmly convinced that the change of working pressure could modulate the content of sp^3-C in a-C:Al films in a certain extent, thereby regulating the hardness and modulus. Compared with pure DLC films reported by other researchers [24,50–52], hardnesses of all the prepared a-C:Al films were at a relatively low level. As mentioned above, Al atoms formed an oxide of aluminum and dissolved into amorphous carbon-based matrix, leading to the distortion of atomic bond angles and the change of carbon bond from sp^3-C to sp^2-C [33,53], which reduced film hardness.

Generally, hardness is an important mechanical property of materials, which has a great influence on wear resistance of films. Plastic resistance index (H/E and H^3/E^2) also can predict the wear resistance of films [54,55]. Fig. 9(b) presents H/E and H^3/E^2 of a-C:Al films fabricated at various working pressures. Both H/E and H^3/E^2 of film at 0.4 Pa reached a maximum of 0.082 and 0.114, respectively. It is of great importance for wear resistance and elastic properties to reach high H/E and H^3/E^2 values [56]. Consequently, the deposited film at 0.4 Pa was expected to possess the best tribological properties among the four a-C:Al samples.

The micrographs of scratch track and critical load of deposited a-C:Al films are presented in Fig. 10. All samples manifest fairly good adhesion strength between films and substrates. What can be seen from Fig. 10(b) is that a-C:Al film deposited at 0.3 Pa presents the highest critical load of about 81 N. And other samples possess similar critical loads (around 75 N). However, Fig. 10(a) shows that the peeled-off area of a-C:Al film expanded at the end of scratch when working pressure ascended from 0.3 Pa to 0.6 Pa. It can be attributed to many factors, such as film thickness, residual stress, hardness, and roughness. In summary, adhesion strength between a-C:Al films and substrates declines as the working pressure rises.

3.5. Tribological behavior

Fig. 11 describes friction coefficient of a-C:Al films against wear time and the inset of Fig. 11 displays an average coefficient of friction as a function of working pressure. Compared with other films, a-C:Al film prepared at 0.5 Pa exhibits the highest friction coefficient of nearly 0.20, while other films perform relatively low friction coefficients in the range of 0.10–0.14. Environment, normal load, and sliding speed have effects on friction coefficient of films [57]. In addition, friction properties are also affected by surface roughness, hardness, adhesion strength and other factors of films [58,59]. Multi factors worked together leading to the irregular change of films' friction coefficient.

As working pressure goes up, wear rates of films firstly goes down and then rises as it is shown in Fig. 12. At working pressure of 0.4 Pa, the film's wear rate has reached a low point of $4.38 \times 10^{-8}\,\mathrm{mm^3\,N^{-1}\,m^{-1}}$. When working pressure continues to rise, wear rate gradually jumps to $10.61 \times 10^{-8}\,\mathrm{mm^3\,N^{-1}\,m^{-1}}$. Undoubtedly, a-C:Al films' mechanical properties and friction coefficient are responsible for wear rates; furthermore, wear resistance is closely relevant to H/E and H^3/E^2 mentioned previously. As a result, a-C:Al film deposited at 0.4 Pa possesses the most outstanding wear resistance.

Wear tracks on a-C:Al films and wear scars on steel balls were characterized. Fig. 13 demonstrates SEM images of wear tracks (a-d) on a-C:Al films and wear scars (e-f) on the corresponding steel ball. All wear tracks presented slight wear with a small amount of wear debris while their corresponding steel balls present big wear scars, implying that the abrasion was mainly performed on steel balls. Compared with other samples, a-C:Al film prepared at 0.4 Pa had the narrowest wear track (189 μm) with the smallest wear scar (287 μm) due to its high hardness and toughness illustrated by the highest value of H/E. The surface profiles of wear tracks are represented in Fig. 14. Wear track depths of the four samples are in the range of 80 nm–230 nm and their changing trend is consistent with the ones of wear rate and wear track morphology. Furrows could be seen on the surface of
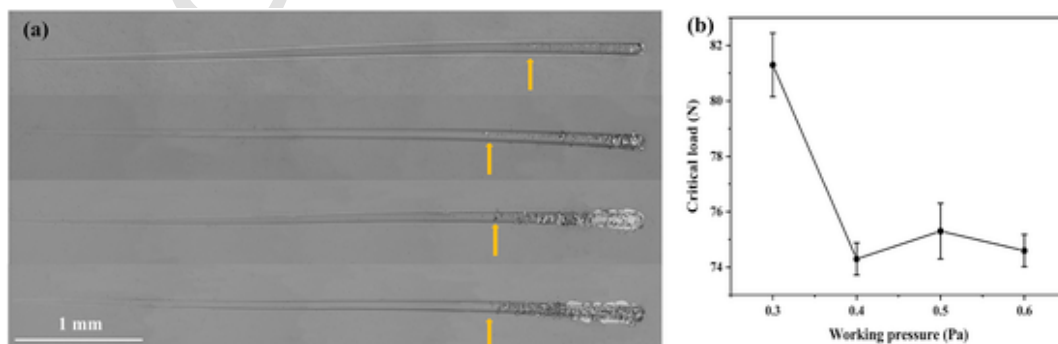

Fig. 10. (a) Micrographs of the scratch track and (b) adhesion curve of a-C:Al films deposited at different working pressures.
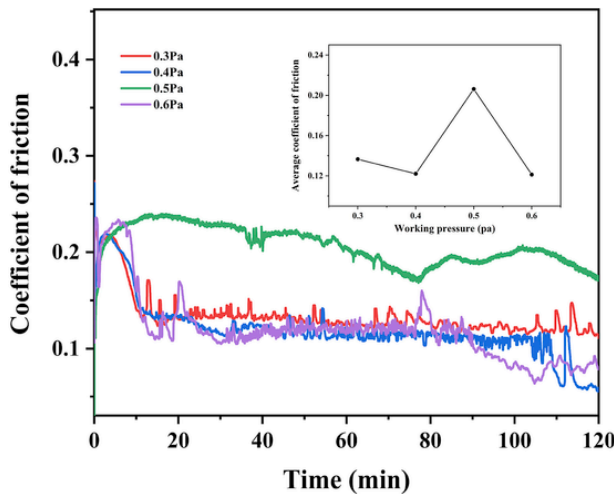
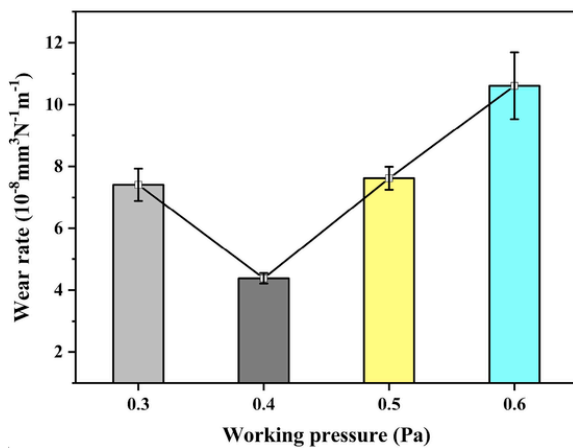**Fig. 11.** Coefficient of friction as a function of wear time.

Fig. 12. Wear rates of a-C:Al films deposited at different working pressures.

C:Al films are in the range of 0.05–0.07. Al/C in wear scar is much higher than that in pristine film, demonstrating that Al gathered on the surface of wear scars and an Al-rich layer formed at friction interface which avoided the direct contact between a-C:Al film and steel ball, contributing to a-C:Al films' excellent wear resistance.

To figure out the change of a-C:Al films' microstructure after wear test, wear scar on steel ball ground against a-C:Al film prepared at 0.4 Pa and wear tracks on four samples prepared at different working pressure were characterized by XPS and Raman, respectively. Fig. 15(a) manifests that the C1s spectrum of wear scar (Fig. 13(f)) was deconvoluted into three peaks: sp^2-C (284.5 eV), sp^3-C (285.1 eV) and C–O (286.5 eV). The ratio of sp^2 content to sp^3 content around 0.69 is higher than that of a-C:Al film which is 0.33 (Fig. 5(b)), indicating that there existed graphitization in wear debris. Fig. 15(b) presents I_D/I_G values of wear tracks and films on cemented carbides. Values of I_D/I_G obtained from wear tracks and corresponding a-C:Al films prepared at 0.4 Pa and 0.6 Pa have little difference, while I_D/I_G values of wear tracks are much lower than that of films deposited at 0.3 Pa and 0.5 Pa, which means that more sp^3-C were produced. Surface materials rearranged its atomic structures and C–C bonds were broken in the sliding interface [60,61]. Dangling bonds on the prepared hydrogen-free a-C:Al films surface generated by friction could be terminated by –H or –OH during wear tests considering the environment humidity of 50% ± 5% according to passivation mechanism [62] which led to the increase of sp^3-C content. Therefore, graphitization in wear debris and passivation of carbon dangling bonds could explain the difference between values of I_D/I_G in wear tracks and the pristine films.

4. Conclusions

The effects of working pressure on structure and properties of a-C:Al films were studied. It was found that atomic composition of Al in a-C:Al films was about 5%, independent of working pressure. Ion current to target, micro-particles collision and ion bombardment to film surface affected film deposition rate as working pressure varied. The prepared films have smooth surfaces with Ra of 2.22 nm–5.89 nm. Typical amorphous structures could be observed in a-C:Al films and sp^3 content could be governed by changing working pressures. Al existed as an oxide of aluminum in carbon matrix. Internal stresses of a-C:Al films were still at a high level of around 2 GPa probably because of the low Al atomic concentration. There was a notable negative correlation between internal stress and sp^3-C content. All samples manifested good adhesion strength to substrates with critical loads beyond 70 N. Wear rates were in 10^{-8} mm^{3}N^{-1} m^{-1} order of magnitude and had the same changing trend with H/E as the working pressure rose from 0.3 Pa to 0.6 Pa.

wear interfaces in Fig. 13(c), (f) and Fig. 14(b), (c) indicating that abrasive wear existed during wear test. Atomic composition of points A, B, C and D in Fig. 13 are described in Table 2. Ratios of Al content to C content (Al/C) at the four points are in the range of 0.11–0.59 while values of Al/C in a-
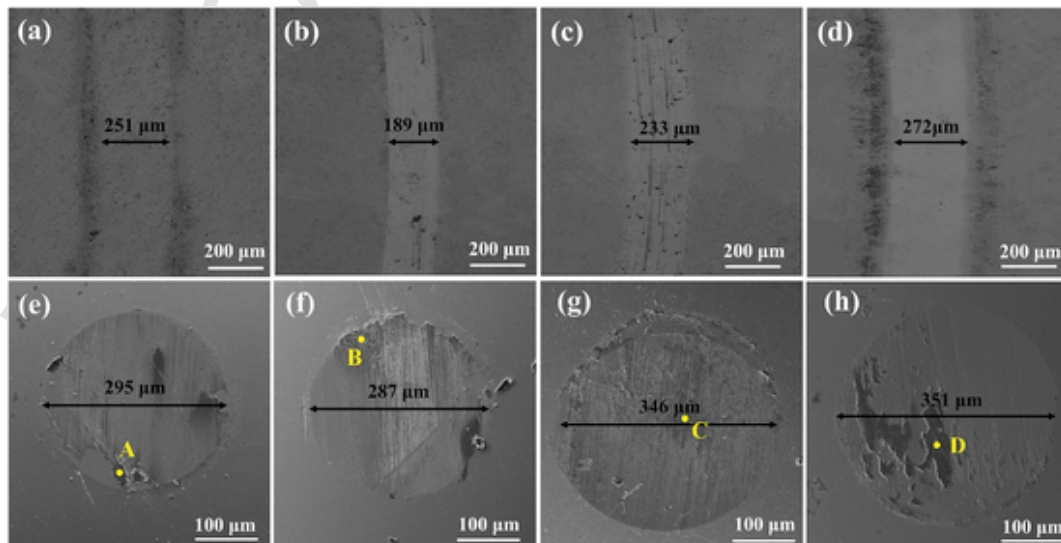

Fig. 13. SEM morphologies of wear tracks of a-C:Al films and wear scars of steel balls: (a) and (e) 0.3 Pa, (b) and (f) 0.4 Pa, (c) and (g) 0.5 Pa, (d) and (h) 0.6 Pa.
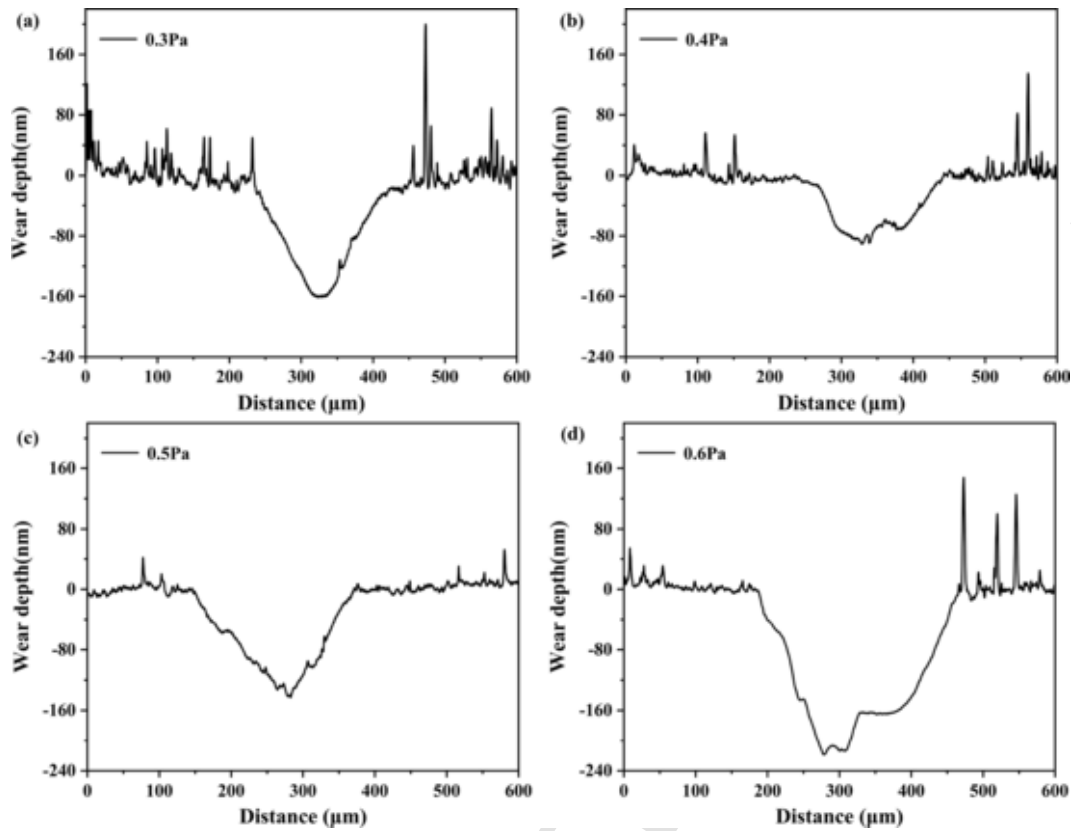
Fig. 14. The surface profiles of wear tracks after friction test (a) 0.3 Pa (b) 0.4 Pa (c) 0.5 Pa and (d) 0.6 Pa.

Table 2
Composition of wear scars on steel balls.

Point	Atomic composition (at. %)						Al/C in wear scar
	C	O	Al	Si	Cr	Fe	
A	21.10	53.75	12.01	0.40	0.27	12.47	0.57
B	23.93	45.17	2.63	0.59	0.64	27.03	0.11
C	20.73	41.82	5.79	0.37	0.54	30.74	0.28
D	34.59	43.37	20.55	0.31	-	1.19	0.59

The lowest wear rate of $4.38 \times 10^{-8} \, mm^3 \, N^{-1} \, m^{-1}$ was obtained for the a-C:Al film deposited at 0.4 Pa.
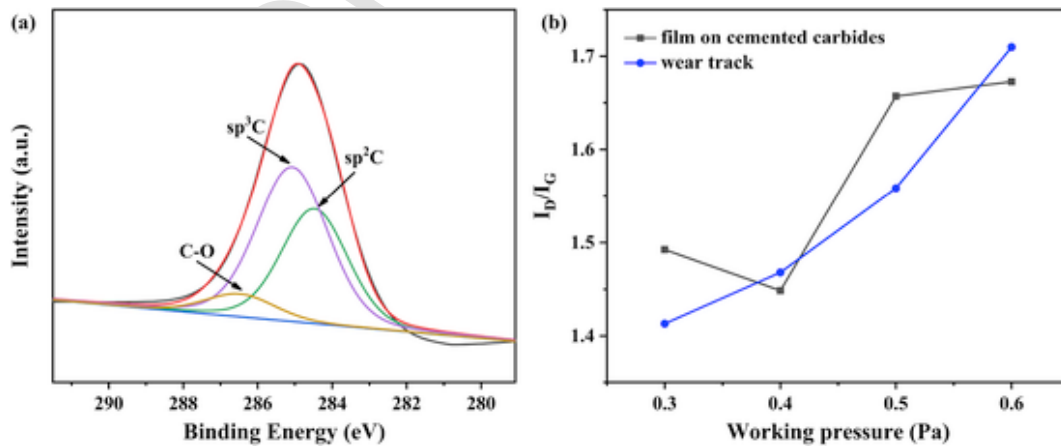
Fig. 15. (a)Deconvolution of C1s XPS spectrum of steel ball wearing against a-C:Al film prepared at 0.4 Pa and (b) I_D/I_G of wear tracks and a-C:Al films on cemented carbides deposited at different working pressure.

References

[1] Y. Chen, J.-M. Wu, X. Nie, S. Yu, Study on failure mechanisms of DLC coated Ti6Al4V and CoCr under cyclic high combined contact stress, J. Alloy. Comp. 688 (2016) 964–973.

[2] P. Safaie, A. Eshaghi, S.R. Bakhshi, Optical properties of oxygen doped diamond-like carbon thin films, J. Alloy. Comp. 672 (2016) 426–432.

[3] S.M. Chiu, S.C. Lee, C.H. Wang, F.C. Tai, C.W. Chu, D. Gan, Electrical and mechanical properties of DLC coatings modified by plasma immersion ion implantation, J. Alloy. Comp. 449 (2008) 379–383.

[4] J. Robertson, Diamond-like amorphous carbon, Mater. Sci. Eng. R Rep. 37 (2002) 129–281.

[5] L. Liu, Z. Wu, X. An, S. Xiao, S. Cui, H. Lin, R.K.Y. Fu, X. Tian, R. Wei, P.K. Chu, F. Pan, Excellent adhered thick diamond-like carbon coatings by optimizing hetero-interfaces with sequential highly energetic Cr and C ion treatment, J. Alloy. Comp. 735 (2018) 155–162.

[6] H. Zhu, T. Zhao, Q. Wei, N. Liu, L. Ma, Z. Hu, Y. Wang, Z. Yu, Corrosion resistance improvement of Mg alloy AZ31 by combining bilayer amorphous DLC:H/ SiNx film with N+ ions implantation, J. Alloy. Comp. 762 (2018) 171–183.

[7] L. Liu, X. An, Z. Ma, Z. Wu, W. Tang, H. Lin, R.K.Y. Fu, X. Tian, P.K. Chu, F. Pan, Hard and adherent a-C:H gradient coatings by stress engineering, J. Alloy. Comp. 765 (2018) 921–926.

[8] L.-Y. Chen, F. Chau-Nan Hong, Diamond-like carbon nanocomposite films, Appl. Phys. Lett. 82 (2003) 3526–3528.

[9] A. Erdemir, O. Eryilmaz, G. Fenske, Synthesis of diamondlike carbon films with superlow friction and wear properties, J. Vac. Sci. Technol. A: Vacuum, Surfaces, and Films 18 (2000) 1987–1992.

[10] X. Li, P. Guo, L. Sun, X. Zuo, D. Zhang, P. Ke, A. Wang, Ti/Al co-doping induced residual stress reduction and bond structure evolution of amorphous carbon films: an experimental and ab initio study, Carbon 111 (2017) 467–475.

[11] S. Zhou, L. Ma, L. Wang, Q. Xue, Tribo-pair dependence of friction and wear moisture sensitivity for aC: Si: Al carbon-based coating, J. Non-Cryst. Solids 358 (2012) 3012–3018.

[12] W. Xu, S. Lin, M. Dai, Q. Shi, C. Wei, X. Zhang, K. Zhou, Effects of bias voltage on the microstructure and properties of Al-doped hydrogenated amorphous carbon films synthesized by a hybrid deposition technique, Vacuum 154 (2018) 159–166.

[13] W. Dai, A. Wang, Deposition and properties of Al-containing diamond-like carbon films by a hybrid ion beam sources, J. Alloy. Comp. 509 (2011) 4626–4631.

[14] N. Cho, K.M. Krishnan, D.K. Veirs, M.D. Rubin, C.B. Hopper, B. Bhushan, Chemical structure and physical properties of diamond-like amorphous carbon films prepared by magnetron sputtering, J. Mater. Res. 5 (1990) 2543–2554.

[15] J. Vetter, 60years of DLC coatings: historical highlights and technical review of cathodic arc processes to synthesize various DLC types, and their evolution for industrial applications, Surf. Coat. Technol. 257 (2014) 213–240.

[16] D.L. Ma, P.P. Jing, Y.L. Gong, B.H. Wu, Q.Y. Deng, Y.T. Li, C.Z. Chen, Y.X. Leng, N. Huang, Structure and stress of Cu films prepared by high power pulsed magnetron sputtering, Vacuum 160 (2019) 226–232.

[17] K. Sarakinos, J. Alami, S. Konstantinidis, High power pulsed magnetron sputtering: a review on scientific and engineering state of the art, Surf. Coat. Technol. 204 (2010) 1661–1684.

[18] K. Sarakinos, A. Braun, C. Zilkens, S. Mráz, J.M. Schneider, H. Zoubos, P. Patsalas, Exploring the potential of high power impulse magnetron sputtering for growth of diamond-like carbon films, Surf. Coat. Technol. 206 (2012) 2706–2710.

[19] S. Nakao, K. Yukimura, H. Ogiso, S. Nakano, T. Sonoda, Effects of Ar gas pressure on microstructure of DLC films deposited by high-power pulsed magnetron sputtering, Vacuum 89 (2013) 261–266.

[20] J.L. Andújar, F.J. Pino, M.C. Polo, A. Pinyol, C. Corbella, E. Bertran, Effects of gas pressure and r.f. power on the growth and properties of magnetron sputter deposited amorphous carbon thin films, Diam. Relat. Mater. 11 (2002) 1005–1009.

[21] G.G. Stoney, The tension of metallic films deposited by electrolysis, Proc. R. Soc. Lond. - Ser. A Contain. Pap. a Math. Phys. Character 82 (1909) 172–175.

[22] Y. Oka, M. Kirinuki, Y. Nishimura, K. Azuma, E. Fujiwara, M. Yatsuzuka, Measurement of residual stress in DLC films prepared by plasma-based ion implantation and deposition, Surf. Coat. Technol. 186 (2004) 141–145.

[23] S. Shiri, P. Ashtijoo, A. Odeshi, Q. Yang, Evaluation of Stoney equation for determining the internal stress of DLC thin films using an optical profiler, Surf. Coat. Technol. 308 (2016) 98–100.

[24] J. Lin, W.D. Sproul, R. Wei, R. Chistyakov, Diamond like carbon films deposited by HiPIMS using oscillatory voltage pulses, Surf. Coat. Technol. 258 (2014) 1212–1222.

[25] P.I.I. Barin, Thermochemical Data of Pure Substances, third ed., 2008.

[26] K.P. Shaha, Y.T. Pei, C.Q. Chen, J.T.M. De Hosson, Synthesis of ultra-smooth and ultra-low friction DLC based nanocomposite films on rough substrates, Thin Solid Films 519 (2010) 1618–1622.

[27] X. Liu, J. Yang, J. Hao, J. Zheng, Q. Gong, W. Liu, Microstructure, mechanical and tribological properties of Si and Al co-doped hydrogenated amorphous carbon films deposited at various bias voltages, Surf. Coat. Technol. 206 (2012) 4119–4125.

[28] E. Fullerton, J. Pearson, C.H. Sowers, S.D. Bader, X.Z. Wu, S. Sinha, Interfacial Roughness of Sputtered Multilayers, Nb/Si, 1994.

[29] V. Zavaleyev, J. Walkowicz, G. Greczynski, L. Hultman, Effect of substrate temperature on properties of diamond-like films deposited by combined DC impulse vacuum-arc method, Surf. Coat. Technol. 236 (2013) 444–449.

[30] R. Dey, M. Pandey, D. Bhattacharyya, D. Patil, S. Kulkarni, Diamond like carbon coatings deposited by microwave plasma CVD: XPS and ellipsometric studies, Bull. Mater. Sci. 30 (2007) 541–546.

[31] G. Zhang, P. Yan, P. Wang, Y. Chen, J. Zhang, The preparation and mechanical properties of Al-containing a-C : H thin films, J. Phys. D Appl. Phys. 40 (2007) 6748–6753.

[32] B. Maruyama, F. Ohuchi, L. Rabenberg, Catalytic carbide formation at aluminium-carbon interfaces, J. Mater. Sci. Lett. 9 (1990) 864–866.

[33] W. Xu, K. Zhou, S. Lin, M. Dai, Q. Shi, C. Wei, Structural properties of hydrogenated Al-doped diamond-like carbon films fabricated by a hybrid plasma system, Diam. Relat. Mater. 87 (2018) 177–185.

[34] D. Wei, K. Peiling, W. Aiying, Influence of bias voltage on microstructure and properties of Al-containing diamond-like carbon films deposited by a hybrid ion beam system, Surf. Coat. Technol. 229 (2013) 217–221.

[35] J. Wang, J. Pu, G. Zhang, L. Wang, Interface architecture for superthick carbon-based films toward low internal stress and ultrahigh load-bearing capacity, ACS Appl. Mater. Interfaces 5 (2013) 5015–5024.

[36] A.C. Ferrari, Determination of bonding in diamond-like carbon by Raman spectroscopy, Diam. Relat. Mater. 11 (2002) 1053–1061.

[37] M. Tamor, W. Vassell, Raman '"fingerprinting"'of amorphous carbon films, J. Appl. Phys. 76 (1994) 3823–3830.

[38] H. Pang, X. Wang, G. Zhang, H. Chen, G. Lv, S. Yang, Characterization of diamond-like carbon films by SEM, XRD and Raman spectroscopy, Appl. Surf. Sci. 256 (2010) 6403–6407.

[39] J. Schwan, S. Ulrich, V. Batori, H. Ehrhardt, S.R.P. Silva, Raman spectroscopy on amorphous carbon films, J. Appl. Phys. 80 (1996) 440–447.

[40] A. Ferrari, J. Robertson, Resonant Raman spectroscopy of disordered, amorphous, and diamondlike carbon, Phys. Rev. B 64 (2001) 075414.

[41] Y. Lifshitz, G.D. Lempert, E. Grossman, Substantiation of subplantation model for diamond-like film growth by atomic-force microscopy, Phys. Rev. Lett. 72 (1994) 2753–2756.

[42] J. Robertson, Deposition mechanisms for promoting sp3 bonding in diamond-like carbon, Diam. Relat. Mater. 2 (1993) 984–989.

[43] X. Li, P. Ke, H. Zheng, A. Wang, Structural properties and growth evolution of diamond-like carbon films with different incident energies: a molecular dynamics study, Appl. Surf. Sci. 273 (2013) 670–675.

[44] B.K. Tay, Y.H. Cheng, X.Z. Ding, S.P. Lau, X. Shi, G.F. You, D. Sheeja, Hard carbon nanocomposite films with low stress, Diam. Relat. Mater. 10 (2001) 1082–1087.

[45] J. Schwan, S. Ulrich, T. Theel, H. Roth, H. Ehrhardt, P. Becker, S. Silva, Stress-induced formation of high-density amorphous carbon thin films, J. Appl. Phys. 82 (1997) 6024–6030.

[46] D. McKenzie, D. Muller, B. Pailthorpe, Compressive-stress-induced formation of thin-film tetrahedral amorphous carbon, Phys. Rev. Lett. 67 (1991) 773.

[47] A.C. Ferrari, S.E. Rodil, J. Robertson, W.I. Milne, Is stress necessary to stabilise sp3 bonding in diamond-like carbon?, Diam. Relat. Mater. 11 (2002) 994–999.

[48] M. Lubwama, B. Corcoran, K. Sayers, J.B. Kirabira, A. Sebbit, K.A. McDonnell, D. Dowling, Adhesion and composite micro-hardness of DLC and Si-DLC films deposited on nitrile rubber, Surf. Coat. Technol. 206 (2012) 4881–4886.

[49] D. Baptista, F. Zawislak, Hard and sp2-rich amorphous carbon structure formed by ion beam irradiation of fullerene, aC and polymeric aC: H films, Diam. Relat. Mater. 13 (2004) 1791–1801.

[50] J. Robertson, Requirements of ultrathin carbon coatings for magnetic storage technology, Tribol. Int. 36 (2003) 405–415.

[51] M. Kamiya, H. Tanoue, H. Takikawa, M. Taki, Y. Hasegawa, M. Kumagai, Preparation of various DLC films by T-shaped filtered arc deposition and the effect of heat treatment on film properties, Vacuum 83 (2008) 510–514.

[52] Y.S. Zou, Y.F. Wu, H. Yang, K. Cang, G.H. Song, Z.X. Li, K. Zhou, The microstructure, mechanical and friction properties of protective diamond like carbon films on magnesium alloy, Appl. Surf. Sci. 258 (2011) 1624–1629.

[53] J.-H. Choi, S.-C. Lee, K.-R. Lee, A first-principles study on the bond characteristics in carbon containing Mo, Ag, or Al impurity atoms, Carbon 46 (2008) 185–188.

[54] N. Oláh, Z. Fogarassy, A. Sulyok, J. Szívós, T. Csanádi, K. Balázsi, Ceramic TiC/a:C protective nanocomposite coatings: structure and composition versus mechanical properties and tribology, Ceram. Int. 42 (2016) 12215–12220.

[55] A. Leyland, A. Matthews, On the significance of the H/E ratio in wear control: a nanocomposite coating approach to optimised tribological behaviour, Wear 246 (2000) 1–11.

[56] S. Dub, Y. Pauleau, F. Thièry, Mechanical properties of nanostructured copper-hydrogenated amorphous carbon composite films studied by nanoindentation, Surf. Coat. Technol. 180–181 (2004) 551–555.

[57] Y. Liu, A. Erdemir, E.I. Meletis, A study of the wear mechanism of diamond-like carbon films, Surf. Coat. Technol. 82 (1996) 48–56.

[58] S. Zhou, L. Liu, L. Ma, Study on structure, mechanical and tribological properties of iron incorporated diamond-like carbon films, J. Non-Cryst. Solids 455 (2017) 35–41.

[59] A. Erdemir, The role of hydrogen in tribological properties of diamond-like carbon films, Surf. Coat. Technol. 146–147 (2001) 292–297.

[60] I.C. Müller, J. Sharp, W.M. Rainforth, P. Hovsepian, A. Ehiasarian, Tribological response and characterization of Mo–W doped DLC coating, Wear 376–377 (2017) 1622–1629.

[61] J. Shi, Z. Gong, Y. Wang, K. Gao, J. Zhang, Friction and wear of hydrogenated and hydrogen-free diamond-like carbon films: relative humidity dependent character, Appl. Surf. Sci. 422 (2017) 147–154.

[62] A.R. Konicek, D.S. Grierson, A.V. Sumant, T.A. Friedmann, J.P. Sullivan, P.U.P.A. Gilbert, W.G. Sawyer, R.W. Carpick, Influence of surface passivation on the friction and wear behavior of ultrananocrystalline diamond and tetrahedral amorphous carbon thin films, Phys. Rev. B Condens. Matter 85 (2012) 543–548.